J MATER RES TECHNOL. 2020;9(4):9195–9205

Available online at www.sciencedirect.com

jmr&t Journal of Materials Research and Technology

www.jmrt.com.br

Original Article

Solid carbon active screen plasma nitrocarburizing of AISI 316L stainless steel in cold wall reactor: influence of plasma conditions

Saeed M. Jafarpour[a,*], *Alexander Puth*[b], *Anke Dalke*[a], *Jan Böcker*[a], *AndreiV. Pipa*[b], *Jürgen Röpcke*[b], *Jean-Pierre H. van Helden*[b], *Horst Biermann*[a]

[a] *Institute of Materials Engineering, Technische Universität Bergakademie Freiberg, Gustav-Zeuner-Str. 5, 09599 Freiberg, Germany*
[b] *Leibniz Institute for Plasma Science and Technology (INP), Felix-Hausdorff-Str. 2, 17489 Greifswald, Germany*

ARTICLE INFO

Article history:
Received 18 March 2020
Accepted 11 June 2020
Available online 30 June 2020

Keywords:
Expanded austenite
Plasma nitrocarburizing
Carbon fibre-reinforced carbon
Active screen technology
Corrosion

ABSTRACT

Low temperature plasma nitrocarburizing processes are widely used surface treatment techniques to improve the surface hardness and wear resistance of stainless steels without loss of their excellent corrosion resistance. In the present study, plasma nitrocarburizing based on the active screen technology was applied in an industrial-scale cold wall reactor for the treatment of AISI 316L. Different technological aspects of a cold wall active screen plasma nitrocarburizing (ASPNC) reactor are addressed. The current study compiles recent achievements for the ASPNC treatment using an active screen made of carbon fibre-reinforced carbon under varying plasma conditions. In addition, it is shown that utilizing an active screen made of carbon opens up the possibility to control the structural properties of expanded austenite by the variation of the plasma conditions. It is revealed that for the ASPNC treatment using an active carbon screen, the high reactivity of the generated plasma at the carbon surface suppresses the requirement to apply a bias discharge.

1. Introduction

Austenitic stainless steels possess great potential for different applications such as chemical and food processing industries due to their superior corrosion resistance [1]. However, their low hardness and poor wear resistance severely limit their applications [2,3]. Low temperature plasma nitrocarburizing (PNC) processes are widely utilized to improve the mechanical and tribological properties of austenitic stainless steels without loss of their excellent corrosion resistance [4–7]. Therefore, the deep understanding of technological and phenomenological aspects of PNC processes to optimize these properties is the object of many scientific studies in past as in current investigations. From the phenomenological aspects in the PNC treatment processes of austenitic stainless steels, both nitrogen and carbon diffuse into the steel surface forming a near surface duplex layer consisting of a nitrogen-enriched layer on top of a carbon-enriched layer known as “expanded austenite” [5–8]. Such a duplex layer combines the high hardness of N-expanded austenite (γ_N) being characteristic for PN layers and the smooth hardness gradient of C-expanded austenite (γ_C) at the layer-core interface being typical for PC layers [5,6]. However, the formation of expanded austenite is only possible at well-defined but very restricted process windows in partic-

* *Corresponding author.*
E-mail: saeed.jafarpour@iwt.tu-freiberg.de (S.M. Jafarpour).
https://doi.org/10.1016/j.jmrt.2020.06.041

ular regarding the appropriate amount of carbon-containing gases to avoid carbon soot formation on the component surface and inside the plasma chamber [5,9]. Besides, the PNC process temperature and duration have great influence on the thermal stability of the expanded austenite. If a temperature-duration threshold is exceeded, the precipitation of chromium nitrides and/or carbides occurs within the expanded austenite resulting in undesired chromium depletion in solid solution of austenite, which reduces the corrosion resistance of the work piece [4,5]. In addition, the structural, mechanical and corrosion properties of generated expanded austenite layer are directly related to the content and diffusion depth of carbon and nitrogen inside the generated expanded austenite. The nitrogen and carbon distribution, in turn, is strongly dependent on the PNC process parameters such as gas mixture, pressure, temperature, time, type of carbon source and plasma parameters [10–12]. Therefore, most research efforts are focused on the variation of the PNC process parameters to optimize the mechanical and structural properties of the expanded austenite [13]. This is conducted in a semi-empirical approach since knowledge of the in situ plasma-chemical conditions, thermo-chemical diffusion interface, and material response is generally not given.

From the technological point of view, conventional PNC processes take place inside a vacuum reactor, by applying a voltage between a cathodic worktable and the anodic reactor wall in a gas mixture of H_2 and N_2 with a low-percentage admixture of CH_4 or CO_2. The applied voltage ionizes the gas mixture. Accordingly, an abnormal glow-discharge forms with a visible glow seam and spreads evenly over the surface of the components to be treated. The charged positive ions are accelerated and impinge on the negatively charged workpieces with a relatively high level of kinetic energy [14]. Generally speaking, a minor fraction of applied energy around 10–20% is required for activation of the chemical reactions and generation of active species, while the large proportion of plasma energy around 80–90% is dissipated in the form of heat to increase the components temperature and to adjust the desired process temperature [15,16]. There are two main types of reactors with respect to the heating source for the PNC processes known as cold wall and hot wall reactors [14,16]. In a conventional cold wall PNC reactor, it is necessary to apply a high plasma voltage (600–800 V) to the components to reach the desired process temperature and maintain the temperature during the PNC process. As a result, some problems like overheating in critical areas such as edges, arcing and a high power consumption are unavoidable [15,17]. In contrast, in a hot wall PNC reactor, which was developed to overcome the problems of cold wall reactor, the components are heated to the process temperature using ohmic heaters placed in the reactor wall. Since the plasma only provides the plasma-chemical conditions, the overall applied plasma voltage (400–500 V) at the components is reduced compared to hot wall PNC reactor [18]. Additionally, hot wall reactors require less time to reach the target temperature and a more *homogeneous* temperature distribution can be obtained compared to cold wall reactors [14]. Furthermore, modern hot wall PNC reactors apply a pulsed dc voltage to reduce or even avoid common problems such as the edge and the hollow cathode effect or a non-homogeneous temperature distribution, all associated with complex geometries [19,20]. However, even for hot wall PNC reactor, the applied plasma voltage at the surface of the components is still high and the previously mentioned issues in cold wall PNC can arise too.

Plasma-assisted thermochemical diffusion treatment processes based on the active screen (AS) technology have been developed to overcome the limitations of conventional plasma-assisted processes by relocating the high-power discharge from the workload to an additionally introduced steel mesh screen, the active screen, which surrounds the worktable and the components to be treated in a cold wall reactor [21–23]. The AS plasma provides (i) the generation of highly reactive gas species from the precursor gases, and (ii) a radiation controlled temperature homogeneity on the work table [24,25]. However, it was shown that a weak bias voltage directly applied to the components surface is essential for large industrial-scale reactors to achieve a beneficial treatment response in case of a steel AS [26,27]. Burlacov and co-workers conducted a study on using the AS technology for plasma nitrocarburizing (ASPNC) processes in an industrial-scale cold wall reactor. By adding different levels of carbon-containing gases such as CO_2 or CH_4 to the H_2-N_2 gas mixture, the specific contribution of the AS plasma responsible for the control of the carburizing potential was identified in case of steel AS [28,29]. Recently, an AS made of a solid carbon material such as carbon fibre-reinforced carbon (CFC) was developed as an alternative to a steel AS [25,30]. It was shown that the generation rates of detectable highly reactive gas species, in particular HCN and C_2H_2, are 30 and 70 times higher for the CFC AS than for the steel AS, respectively [31,32]. In case of AS made of CFC, recently the influence of the N_2-H_2 gas composition on the structure and properties of expanded austenite was studied using AISI 316L stainless steel [25]. However, an in-depth investigation regarding the effect of bias conditions on the ASPNC treatment of AISI 316L stainless steel using a CFC AS and on the resulting properties is required.

In the present study, the influence of the bias plasma power at the component as well as AS plasma power on the structural properties of ASPNC treated AISI 316L austenitic stainless steel using an AS made of CFC in a cold wall reactor was investigated. Therefore, a specially designed sample holder was used [29] to provide a simultaneous treatment of both sides of a sample disk at different plasma conditions. The variations of structural, mechanical and corrosion properties of AISI 316L steel after the PNC treatment with an AS made of CFC were investigated using optical light microscopy, X-ray diffraction (XRD) analysis, glow discharge optical emission spectroscopy (GDOES), scanning electron microscopy (SEM), microhardness measurement and potentiodynamic polarization tests.

2. Material and methods

The austenitic stainless steel grade AISI 316L (wt.%: C 0.05, Cr 17, Ni 11.4, Mo 1.9, Mn 1.5, Si 0.35 and Fe balance) was used for the investigation. Samples of 20 mm in diameter and 5 mm in thickness were machined from a commercial cylindrical bar. Sample with surface finishing of wet ground up to 800 SiC paper grid was prepared, cleaned with ethanol in an ultrasonic bath and dried in hot air prior to the ASPNC treatment.

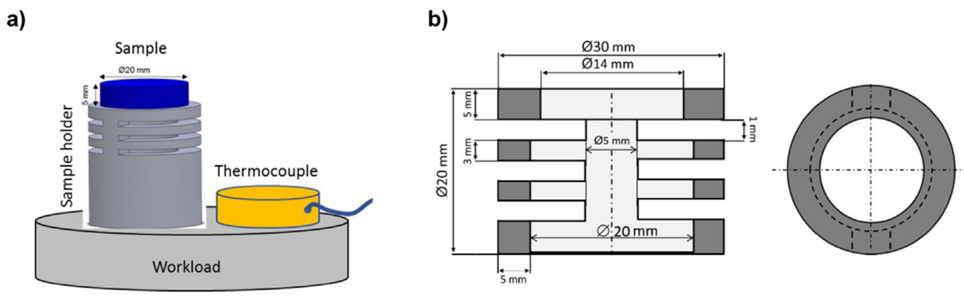

Fig. 1 – Schematic of the mounted sample on sample holder (a) and its dimensions (b).

The sample holder (Fig. 1a) provides a simultaneous treatment of both sides of a sample disk under two different bias plasma conditions: (i) with the variable bias plasma exposure at the front-side and (ii) without bias plasma exposure, i.e. in the pure afterglow at the back-side. Several radial narrow slits with 1 mm width and a distance between two slits of 3 mm in the cylindrical sample holder provided a flow of the active species to the back side of the sample during the process (Fig. 1b). Such a treatment at the two different bias plasma conditions can be considered as an initial realization for bulk treatment of components.

In an industrial-scale cold wall ASPNC reactor with a vacuum chamber size of 1 m in diameter and 1 m in height as well as CFC AS in the middle with 800 mm in diameter and 750 mm in height [25,30], two types of processes were performed. First, ASPNC processes without samples were conducted to investigate the effects of crucial parameters such as process temperature, bias power, and gas composition on the AS power. This defines the reactor response. Second, ASPNC processes were performed with AISI 316L austenitic stainless steel samples placed on the sample holder to investigate the effect of AS power and bias power variations on the structural, mechanical and corrosion properties of treated sample. In turn, this defines the treatment response. The process started by evacuating the reactor to a base pressure of $p = 0.8$ mbar. Subsequently, a hydrogen-nitrogen gas mixture with a ratio of H_2:N_2 = 1:1 at a total flow rate of $\Phi = 60$ slh was introduced into the reactor at $p = 1.6$ mbar pressure and the main power supply was turned on to generate the discharge at the CFC AS for heating up the worktable and samples. After reaching a temperature of 250 °C, measured with thermocouples placed at the workload, different bias powers were adjusted until the temperature of the samples reached 430 °C. Then, the total flow rate of the H_2-N_2 gas mixture with ratio of H_2:N_2 = 1:1 was increased to $\Phi = 80$ slh and the pressure was increased to $p = 3$ mbar. After the desired process temperature of 460 °C was reached within 45–60 min depending on the bias power values, the set process parameters were maintained (H_2:N_2 = 1:1, $\Phi = 80$ slh, $p = 3$ mbar) for 5 h to perform treatment process. Finally, after 2 hours of cooling process under 20 slh H_2, the samples were removed from the reactor.

The surface topography of the treated samples was investigated on a MIRA3 TESCAN scanning electron microscope (SEM). The cross sections of the ASPNC treated samples were metallographically polished and chemically etched with Beraha II etchant to study the microstructure and to assess the thickness of the expanded austenite layer using a Carl Zeiss Neophot 30 optical light microscope equipped with a JVC TK C1381CCD-camera and the Image C/A4i analysis software. Microhardness-depth profile measurements were conducted at a LECO M-400G3 equipped with a Knoop micro indenter applying a load of 10 g. The phases present in the treated samples were analyzed by X-ray diffraction (XRD) with a URD6 (SEIFERT-FPM) diffractometer operated at $U = 40$ kV and $I = 30$ mA. A conventional θ–2θ Bragg-Brentano symmetric diffraction geometry with CoKα ($\lambda_1 = 1.78897$ Å, $\lambda_2 = 1.79285$ Å) radiation was used. The diffractogram was recorded in an angular range from 20° to 150° with a scan rate of 0.7°/min realized by Dectris Meteor 1D detector. In addition, ASPNC treated samples were analyzed by GDOES on a LECO SDP 750 spectrometer to determine the concentration-depth profiles of nitrogen, carbon, and other elements after ASPNC. The corrosion behaviour was examined by potentiodynamic polarization in a 0.05 M H_2SO_4 solution using a conventional three-electrode configuration with the sample as the working electrode, a saturated Ag/AgCl electrode as reference and a platinum mesh as the counter electrode. The scan rate was 6 mV/min.

3. Results and discussion

3.1. *Technological aspects of ASPNC process in a cold wall reactor*

It was shown by Puth et al. that the concentrations of the detected molecular reaction products depend on the AS plasma power in a cold wall ASPNC reactor using CFC AS [31]. Hence, investigation of the AS plasma power variation as a function of crucial ASPNC process parameters is one of the key points for controlling the concentrations of molecular reaction products. Therefore, the first set of processes was performed to realize the effect of ASPNC process parameters such as temperature, gas composition and bias plasma power on the AS plasma power using CFC AS without inserting any samples (reactor behaviour). Without bias plasma at the components, the AS plasma power is regulated based on a constant process temperature. It was shown that the AS plasma power increases by increasing the temperature as higher AS plasma power is needed to reach the higher process temperature (Fig. 2a). In addition, it was revealed that the variation of the H_2-N_2 gas mixture has a significant influence on the AS power in cold wall ASPNC reactors (Fig. 2b). Increasing the

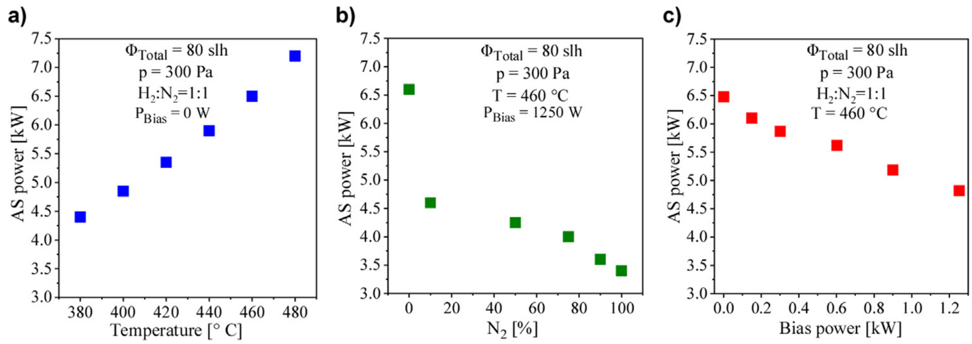

Fig. 2 – Technological dependencies of AS power on the temperature (a), gas composition (b) and bias power (b) using CFC AS in a cold wall ASPNC reactor.

Table 1 – Concentrations of active species for the ASPNC process in the industrial-scale cold wall reactor without and with bias power at 500 °C temperature using a CFC AS [25,33].

Gas composition	Plasma conditions (kW)		Concentration (10^{15} cm^{-3})		
	P_{bias}	P_{AS}	HCN	NH_3	CH_4
H_2:N_2 = 1:1 (80 slh)	0	7.8	5.5	1.5	2
H_2:N_2 = 1:1 (80 slh)	1.25	4.6	3	0.8	0.3

N_2 in the H_2-N_2 gas mixture led to a strong decrease in AS plasma power. Moreover, in case of applying a bias voltage to the components, it was observed that the AS plasma power was reduced due to the additional heat inserted by the bias plasma power (Fig. 2c). In this case, both the AS power and the bias power are responsible for heating up the samples and adjusting the process temperature. In order to further support the above findings, evidences for the strong dependency of the AS power and resulting active species concentrations on the bias conditions were selected from Dalke et al. [25] and Puth et al. [33]. There, infrared laser absorption spectroscopy (IRLAS) was used to determine the concentrations of C_2H_2, CH_4, HCN, and NH_3 during ASPNC using a CFC AS under non-biased and 1.25 kW biased conditions at 500 °C temperature in the same cold wall reactor used in this study. Comparing these two investigations [25,33], it is concluded that by increasing the bias power from 0 W to 1.25 kW, the AS power decreased from 7.8 kW to 4.6 kW. As a result of decreasing AS power, the chemical sputtering of the solid carbon source as well as the concentrations of important process-relevant species such as HCN, NH_3, C_2H_2, and CH_4 decreased (Table 1) [31].

3.2. *Effect of plasma condition on the structural properties of treated samples*

The sample holder (Fig. 1) was utilized for ASPNC of AISI 316L to simultaneously treat both sides of a sample disk under two different plasma conditions. Fig. 3 shows selected cross-sectional optical micrographs captured from the front and the back side of ASPNC treated samples. It is shown, that for all investigated conditions a dual-layer consisting of nitrogen-expanded austenite γ_N on top of a carbon-expanded austenite γ_C is formed on both sides of the treated samples. The driving force behind the duplex layer formation is a difference between the diffusion coefficients of carbon and nitrogen atoms in the crystalline structure of austenitic stainless steels as well as the so called pushing effect of nitrogen on carbon interstitial atoms [8,34]. This dual-layer is more homogeneous along the surface at the front side compared to the back side and the thicknesses of γ_N and γ_C depend on the bias power and the AS power as well as the concentrations of active species.

Fig. 4 shows the thicknesses of γ_N and γ_C layers as well as the entire layer thickness $\gamma_N + \gamma_C$ as a function of the AS power and the bias power, estimated by light optical microscopy measurement of etched cross sections. At the front side of the treated sample without bias power, the thicknesses of γ_N and γ_C are roughly identical $\gamma_N \cong \gamma_C \cong 8\,\mu m$ (Fig. 3a). At a low bias power condition of 0.15 kW on the front side where a plasma glow seam was formed, the thickness of γ_N is increased up to 12 µm, while the thickness of γ_C is reduced to 4 µm. The ratio of γ_N/γ_C as well as the total thickness of expanded austenite $\gamma_N + \gamma_C$ is comparable for all five examined bias power settings ranging from 0.15 to 1.25 kW. Puth et al. [31] showed that in ASPNC process using CFC AS, the reduction of AS plasma power led to the reduction of active species concentrations. However, in our investigated AS power range, it can be supposed that the concentrations of active species are still sufficiently high to produce comparable total layer thicknesses of the resulting expanded austenite (Fig. 3a). The generation of active species in case of CFC AS is generally related to the chemical sputtering during plasma-solid carbon interaction at the AS [35] which results in a much higher production rate of volatile products at low threshold energy (several eV) in contrast to physical sputtering [36].

Due to the design of the sample holder, no plasma glow seam was formed at the back side of the treated samples in case of biased condition. At the back side, in the case no bias voltage (P_{Bias} = 0 W) was applied (Fig. 4b), the total layer thickness decreased compared to the front side of sample for the comparable bias condition (highlighted by green in Fig. 4a and b). However, the thickness ratio of γ_N/γ_C remained identical. For the back side of the treated samples where different bias voltage values (P_{Bias} = 0.15–1.25 kW) were applied (Fig. 4b), the thickness of γ_N and γ_C are also roughly identical $\gamma_N \cong \gamma_C$. However, by increasing the bias power which means the AS power is decreasing, the total thickness of expanded austenite $\gamma_N + \gamma_C$ decreased.

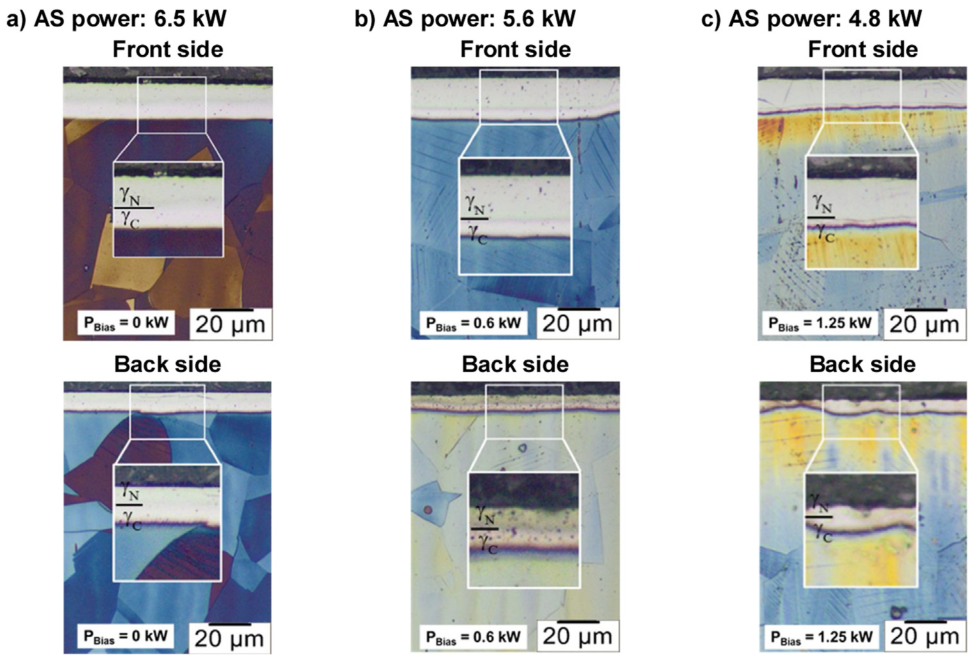

Fig. 3 – Cross-sectional optical micrographs captured from front side and back side after ASPNC treatment at different plasma conditions showing expanded austenite layer (etchant: Beraha II reagent).

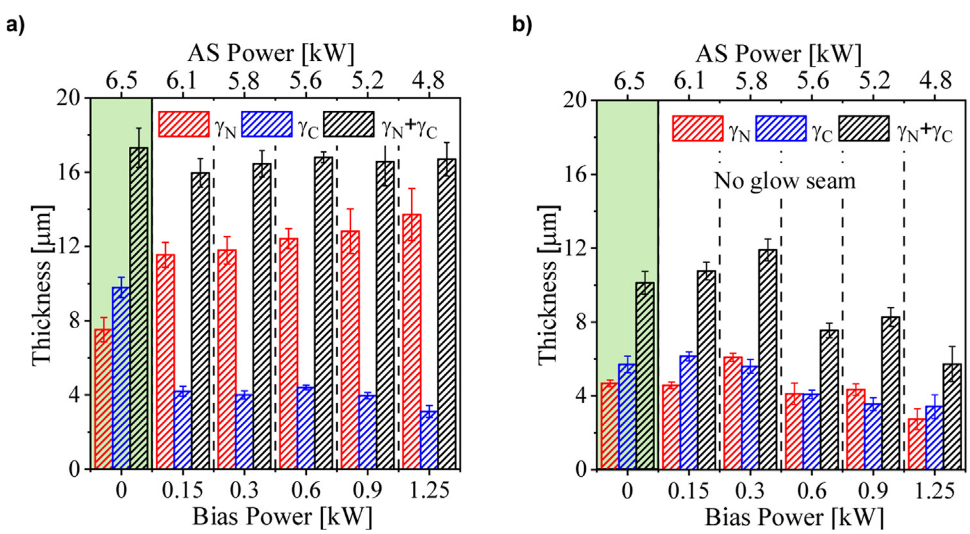

Fig. 4 – Thickness of nitrogen-expanded austenite γ_N and carbon-expanded austenite γ_C as well as the entire layer thickness $\gamma_N + \gamma_C$ as a function of the AS power and the bias power measured at cross sections for front side (a) and back side (b) of ASPNC treated samples (non-biased conditions at the front side and the back side of a sample are highlighted by green).

Fig. 5 shows schematics of ASPNC processes at biased and non-biased conditions. Generally, for the ASPNC process using a CFC AS without applying a bias voltage at the components (Fig. 5a), the process is characterized by the mechanisms of the afterglow nitrocarburizing [37]. In this afterglow process, the main detected reaction products are CH_4, C_2H_2, NH_3, HCN, and CO where HCN is the most important species due to its dual ability for (i) an activation of the passivated surface in order to remove the chromium oxide passive film, and (ii) the supply of both carbon and nitrogen for ensuring the diffusion of both elements during nitrocarburizing treatment of stainless steels [32]. Considering all influencing variables, e.g. H_2-N_2 gas mixture, pressure, temperature and time that are constant in this work, the generation of HCN mainly depends on the AS plasma power (Table 1). Here, in case of ASPNC treatment without applied bias, the AS plasma power had its maximum value at about P_{AS} = 6.5 kW, and it continuously decreased by increasing the bias plasma power at the samples (Fig. 2b). The AS plasma power reached its minimum value P_{AS} = 4.8 kW in case of the maximal bias power of P_{Bias} = 1.25 kW. It is proposed

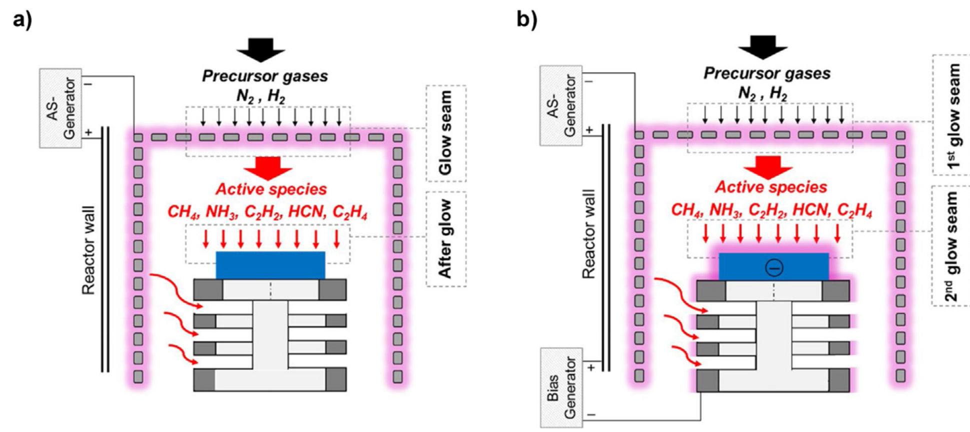

Fig. 5 – Schematics of two different processes using non-biased (a) and biased (b) conditions at the sample and sample holder.

that even at a low AS plasma power of $P_{AS} = 4.8$ kW, a sufficient concentration of HCN was produced to generate a similar thick layer of expanded austenite like in the case of a high AS plasma power ($P_{AS} = 6.5$ kW) at the front side of the treated samples (Fig. 5a). In addition, it is shown that in case of the non-biased condition, the total thicknesses of expanded austenite significantly decreased at the back side compared to the front side of the treated samples. It can be proposed that in case of non-biased condition, the concentration of active species resulting from the interaction of AS plasma and CFC surface were decreased at the back side due to the narrow slits with 1 mm width in the cylindrical sample holder compared to the front side.

Comparing the cross-sectional optical micrographs of the biased samples with the non-biased sample at the front sides (Fig. 3), it can be proposed that the increase of the thickness of nitrogen-expanded austenite γ_N is due to the fact that, in addition to carbon and nitrogen from HCN, positive ions have significant influences on the thickness of nitrogen-expanded austenite γ_N. Different positive ions such as N^+, NH^+, $NH_2{}^+$, $NH_3{}^+$, $NH_4{}^+$, $N_2{}^+$ produced in the glow seams [38] can be attracted by the negatively charged (biased) sample surface (Fig. 5b). In addition, it is also revealed that the thickness of nitrogen-expanded austenite γ_N is independent on the amount of bias power as roughly identical thickness of γ_N was achieved for different values of bias powers at the front side of the treated samples.

In addition, comparing the biased condition at the front side and the back side of treated samples (Fig. 5b), the total thicknesses of expanded austenite decreased at the back side compared to front side (Fig. 5). There are two different reasons for such a behaviour at the back side at biased condition. First, it is proposed that the AS plasma power as well as the resulting active species concentrations decreased due to the increase of bias power at the front side (Fig. 2c). In addition, the concentrations of active species in particular positive ions can be further decreased at the back side as they were attracted by front side of the sample as well as sample holder in addition to the reduction due to the narrow slits with 1 mm width in the sample holder.

Microhardness-depth profiles measured from the surface to the core on the front side (Fig. 6a) and back side (Fig. 6b) of ASPNC treated samples are shown in Fig. 6. In all cases, in the expanded austenite the hardness decreased gradually from the surface towards the core, such that a gradient hardness profile results, which is a characteristic for PNC treatments of stainless steels. From Fig. 6a, it was revealed that at the front side of ASPNC treated samples, a maximum hardness value of around 1400 HK 0.01 was achieved without bias power. As the negative bias was applied to the samples, the hardness value increased up to 1700 HK 0.01 and remained constant for different bias powers. In contrast, at the back side of ASPNC treated samples (Fig. 6b), the hardness was influenced by a significant decrease of the AS power which is correlating with a reduction in active species concentrations. Accordingly, for the lowest AS power of about 4.8 kW and the associated low concentrations of active species at the back side of samples, a minimum expanded austenite layer thickness of around 6 μm as well as a low hardness value of around 600 HK 0.01 were measured. The maximum hardness of about 1350 HK 0.01 measured at the back side of the samples was achieved for a AS plasma power of 5.8 kW which is related to the thicker expanded austenite layer (around 10 μm) for this condition. In addition, the results of microhardness-depth profile measurements at the front and back side of examined samples (Fig. 6) are directly correlated with the thickness measurement of γ_N and γ_C layers (Fig. 4). Generally, in case of the ASPNC process, high interstitial content of atomic carbon and nitrogen is obtained due to the relatively strong affinity of N atoms and to a lower extent of C atoms for Cr, leading to a short-range ordering of Cr and nitrogen or carbon. Due to the low mobility of Cr atoms as compared to interstitial nitrogen and carbon atoms at the treatment temperature, chromium nitrides or carbides do not precipitate until after long exposure times according to stability curve thus thermochemically diffused nitrogen and carbon are kept in solid solution and cause the expansion of austenitic lattice [12,34]. The expansion of the austenitic lattice parameter is responsible for the increase of compressive residual stresses in this phase, which together with solid solution hardening result in an increased hardness at the surface of expanded austenite.

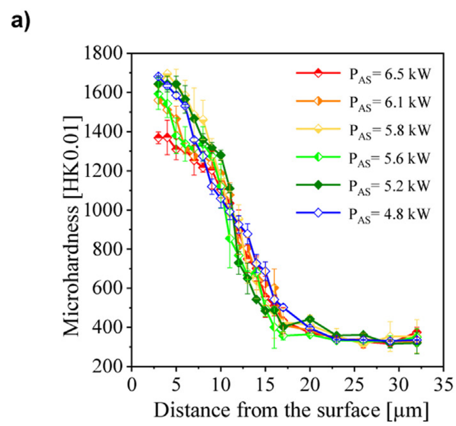

Fig. 6 – Microhardness-depth profiles for different plasma conditions measured at the front side (a) and back side (b) of ASPNC treated samples with an AS made of CFC (red colour indicates the P_{Bias} = 0 W).

3.3. *Effect of bias power variation on the properties of expanded austenite*

3.3.1. *Structural and compositional analysis*

Due to the weak structural and mechanical properties of expanded austenite at the back side of ASPNC treated samples, further investigations were conducted only at the front side of ASPNC treated samples. Fig. 7a shows the X-ray diffraction patterns for an untreated and for treated AISI 316L samples. For the untreated AISI 316L, two characteristic peaks were observed at angles of 51.1° and 59.7°, corresponding to face centred cubic (fcc) γ(111) and γ(200) peaks of austenitic stainless steel, respectively. In case of ASPNC treated samples at biased condition, two defined peaks of the metastable nitrogen-expanded austenite, indicated at γ_N(111) and γ_N(200), appear at lower shifted angles of around 47.2° and 53.6° compared to untreated samples, respectively. In addition, it is revealed that the peak positions are roughly similar for samples treated at different bias powers. Moreover, compared to the untreated fcc austenite peaks, a broadening of the peaks is observed [39,40]. It is worth to mention here that due to the high thickness of nitrogen-expanded austenite of $\gamma_N \cong 12\,\mu m$ in case of biased samples, the carbon-expanded austenite peak is only visible for the sample treated at non-biased condition, at which a thickness value of only 8 µm is measured for γ_N (Fig. 7a). For the sample treated at non-biased condition, two defined peaks of the metastable nitrogen-expanded austenite, indicated as γ_N(111) and γ_N(200), appear at lower shifted angles of around 48.2° and 54° compared to untreated sample, respectively. It is shown that for non-biased condition, the diffraction peaks attributed to the γ_C phase are closer to the lines related to the untreated γ phase than those from the γ_N phase. This is explained by the lower carbon content in expanded austenite compared to nitrogen. The shift to the left and the anisotropic broadening of the diffraction peaks in expanded austenite can be explained by both the expansion of the fcc lattice and the formation of compressive stresses that build up in the surface layer due to the high nitrogen content introduced during the ASPNC [41].

Fig. 7b shows the concentration-depth profiles of nitrogen and carbon measured by GDOES analysis on the front side of samples treated at different bias plasma powers. The graphs show the nitrogen concentrations ranging from 0 to 20 wt.% and the carbon concentrations ranging from 0 to 5 wt.%. At non-biased condition, a carbon content of 2 wt.% and a nitrogen content of 10 wt.% were measured. As a low bias power (0.15 kW) was applied to the sample, the nitrogen content at the surface increases to around 20 wt.% while carbon content decreases to 1.5 wt.%. The increase in the nitrogen content for biased samples compared to the non-biased sample is because positive ions were attracted by the negatively charged (biased) samples in addition to carbon and nitrogen from HCN. In addition, it is shown that by increasing the bias plasma power from 0.15 kW to 1.25 kW, the nitrogen and carbon contents did not change. However, there was a slight increase in diffusion depth of atomic nitrogen observed at a nearly constant total case depth. These results are in good agreement with the results obtained for the thickness of γ_N and γ_C for biased and non-biased conditions at the front side of treated samples (Fig. 4a).

3.3.2. *Surface topography analysis*

Fig. 8 shows the surface topography captured by SEM in two different magnifications of samples treated with different bias plasma powers. At non-biased condition, a uniform layer develops on the surface of the austenitic steel and no grain boundary effects are visible (Fig. 8a). However, in the case where a bias voltage was applied to the sample, grain boundary effects were observed on the surface as indicated by white arrows (Fig. 8b and c). This can be explained by the highly distorted expanded austenite, as the presence of the interstitial elements, e.g. in particular nitrogen, is above the solubility limit. During ASPNC processes, the distortion of the lattice causes the formation of compressive residual stresses with the consequence of the development of defects inside the grains like stacking faults, sliding bands, twins etc., which generate asymmetric strains according to different crystallographic orientations [39–41]. To avoid these undesired effects, it is necessary to reduce the nitrogen content in the γ_N layer and thus to preserve the surface state of the treated samples as observed for the case without bias power. In addition, high magnification SEM images revealed the formation of nano-

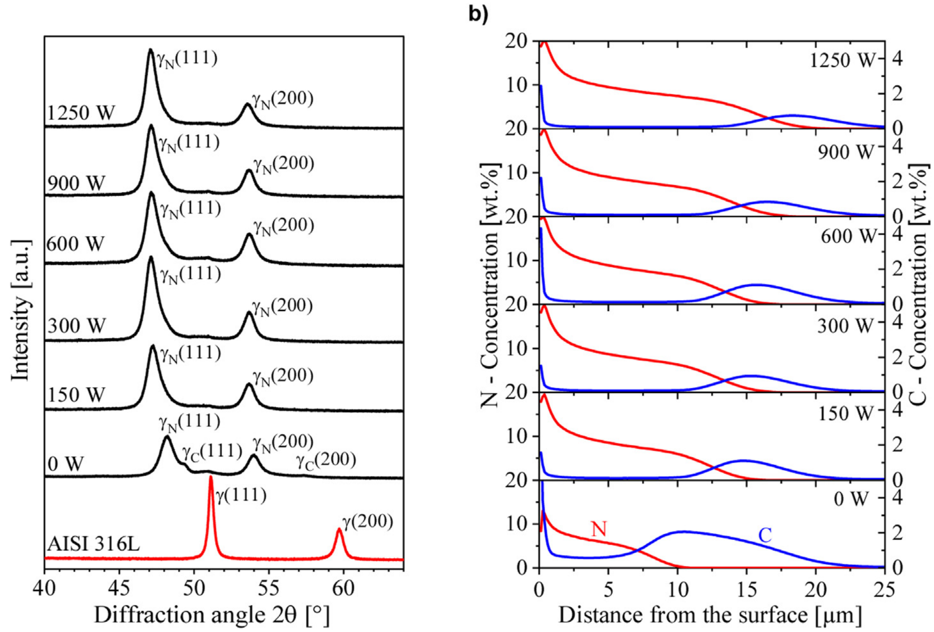

Fig. 7 – X-ray diffraction patterns (a) and GDOES concentration depth profiles of nitrogen and carbon (b) measured at the front side of ASPNC treated samples under variation of the bias power.

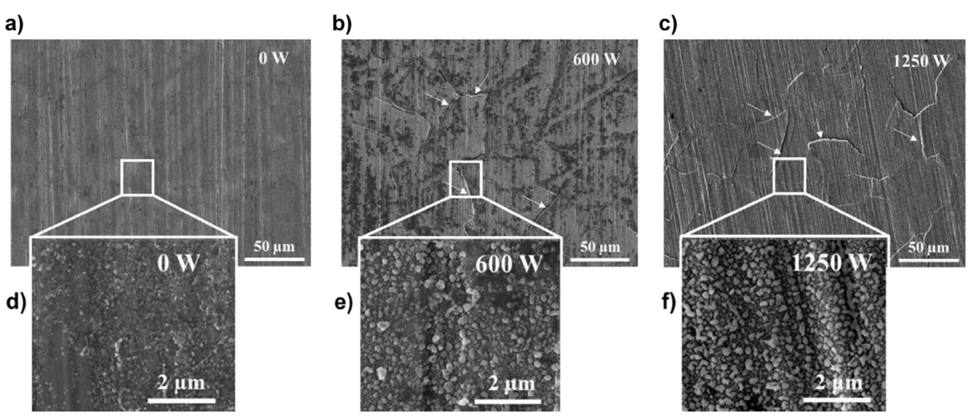

Fig. 8 – Surface topography (SEM) of ASPNC treated samples for different plasma conditions: (a, d) P_{Bias} = 0 W, P_{AS} = 6.5 kW; (b, e) P_{Bias} = 600 W, P_{AS} = 5.6 kW; (c, f) P_{Bias} = 1250 W, P_{AS} = 4.8 kW at two different magnifications.

sized particles on the surface of the ASPNC treated samples in case of biased samples (Fig. 8e and f) while without bias power, the density of these particles is significantly lower (Fig. 8d). It can be proposed that the formed nanoparticles at the surface are iron nitride, carbide and carbonitride as well as chromium nitride as suggested by other researchers [17,42]. The formation of these nanoparticles could be attributed to sputtering of iron and chromium from the initial steel surface, which react with carbon and nitrogen active species, and are re-deposited on the sample surface under bias condition. The formation of chromium carbide, however, is not favourable at the applied process temperature [15,42].

3.3.3. *Corrosion behaviour*

In order to further characterize the influence of the expanded austenite layers generated by different bias plasma powers, their passivation behaviour was investigated by means of potentiodynamic polarization tests in a 0.05 M H_2SO_4 electrolyte (pH = 1.4). The results are presented in Table 2 and Fig. 9. For both untreated and ASPNC-treated samples, a comparable corrosion potential E_{cor} in the range of about −0.5 mV was determined (Fig. 9). With increasing polarization, however, the passivation behaviour of ASPNC treated samples differs significantly from that of the untreated base material. Generally, the ASPNC treated samples undergo an accelerated corrosion characterized by the increased passivation current density i_P, but they passivate faster as they reach the passive state at lower potentials compared to the untreated material (Table 2). Flis [43] attributed the fast passivation to accumulation of protective corrosion products as the existing passive layer on nitrided stainless steels contains small amounts of oxygen containing species on top and Cr-N species in deeper regions. For the comparison of the passive current density i_{pass}, that describes the protective effect of the passive layer, a potential in the passive state at +500 mV was chosen (Table 2). For the

Table 2 – Corrosion parameters of the untreated and ASPNC treated AISI 316L at different bias powers tested in 0.05 M H_2SO_4 solution.

P_{Bias} (kW)	E_{cor} (V)	i_{pass} (mA/cm^2)	E_P (V)	i_P (mA/cm^2)	N (wt.%)	C (wt.%)
Untreated	−0.320	0.0025	0.25	0.016	–	–
0	−0.322	0.007	0.1	0.17	12	5
0.6	−0.336	0.02	−0.20	0.21	20	4
1.25	−0.352	0.035	−0.15	0.1	20	2

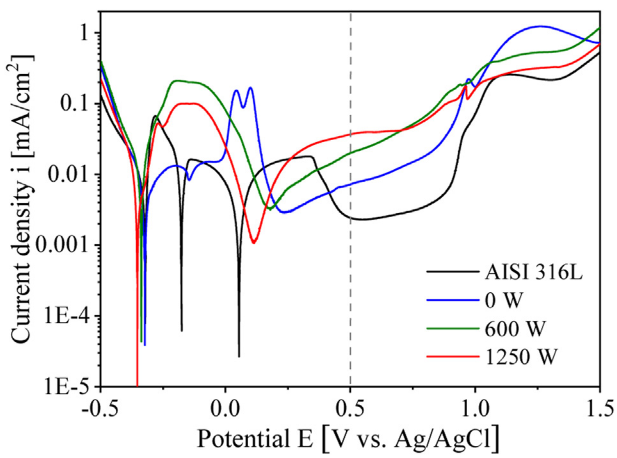

Fig. 9 – Potentiodynamic anodic current density/potential curves measured at untreated and ASPNC treated AISI 316L samples at different bias plasma power settings.

ASPNC treated sample conditions, the passive current densities i_{pass} increased by a factor of 3 for the unbiased condition up to a factor of 14 for the biased samples compared to the untreated material (Table 2). This indicates a lower protective effect of the passive layer on nitrocarburized samples against an acidic solution that correlates to literature data for low temperature thermochemical treated austenitic stainless steels [12,43–45]. Nevertheless, the differences in the dissolution rate, expressed in the higher passive current density i_{Pass}, observed between the biased and unbiased condition could be a result of the different surface states concerning the nitrogen and carbon contents present at the surface (Table 2). For the unbiased sample, the transition between the active/passive area starts later compared to the biased samples. While in the initial range up to a potential of 0 V a very low current density is present, this increases abruptly up to the passivation current density i_P. Since the amount of nitrogen within the nitride layer has a great influence on the corrosion results [45], the correlation of the surface properties, e.g. type and phase composition of the particles, with the ASPNC parameters is essential. In accordance with the surface morphologies and the observed presence of particles (Fig. 8), the influence of Cr-N and/or Cr-C compounds formed at the surface will be considered in future investigations.

4. Conclusions

Different technological aspects of ASPNC with CFC AS were addressed to perform a reliable treatment in an industrial-scale cold wall reactor. Hence, the AS plasma power was characterized as a function of set temperature, H_2-N_2 feed gas composition and bias plasma power. It was shown that each of these process parameters has a strong influence on the AS plasma power which can be correlated to the concentrations of important active species. In addition, the change in the AS plasma power as a function of the bias plasma power in wide ranges as well as utilizing a specially-designed sample holder allowed the investigation of different conditions for sample treatment. It was demonstrated that in the case a bias voltage was applied to the samples with a glow seam formation, additional nitrogen from positive ions was attracted by the negatively charged samples in addition to carbon and nitrogen from HCN. Therefore, without bias power, the thicknesses of γ_N and γ_C are comparable while for biased samples, γ_N is thicker than γ_C. The concentration of HCN as a result of the different plasma conditions can be correlated with the structural changes of the expanded austenite. This finding emphasizes the importance of controlling the plasma-chemical conditions in plasma-assisted nitrocarburizing processes to optimize both nitrogen and carbon uptake in austenitic stainless steel. The present study demonstrates that for PNC treatment using a carbon AS, the effect of both bias and AS plasma powers process parameters are crucial influencing the resulting materials surface properties. Beyond that, it also shows that due to the high reactivity of the plasma-chemical environment generated by use of the carbon AS, the use of a bias is optional, which in turn may enable the ASPNC treatment of bulk materials. Furthermore, for the deep understanding of the effect of the process parameters on the sample response, localized and near surface spectroscopic investigation is required in future work.

Conflicts of interest

The authors declare no conflicts of interest.

Acknowledgements

The authors appreciate the Federal Ministry of Education and Research (BMBF) for financial support in the framework of the validation funding VIP+ in the project PNC-Control, project numbers 03VP05501 and 03VP05502. The authors thank Dr. Ch. Schimpf (TU Bergakademie Freiberg, Institute of Materials Science) for XRD analysis, Dr. M. Mandel (TU Bergakademie Freiberg, Institute of Materials Engineering) for potentiodynamic polarization tests and Ms. I. Diegel (TU Bergakademie Freiberg, Institute of Materials Engineering) for metallographic preparation.

REFERENCES

[1] Lo KH, Shek CH, Lai JKL. Recent developments in stainless steels. Mater Sci Eng: R: Rep 2009;65(4):39–104.
[2] Bell T. Surface engineering of austenitic stainless steel. Surf Eng 2002;18(6):415–22.
[3] Zhang ZL, Bell T. Structure and corrosion resistance of plasma nitrided stainless steel. Surf Eng 1985;1(2):131–6.
[4] Sun Y, Haruman E. Low temperature plasma surface alloying of austenitic stainless steels. SSP 2006;118:85–90.
[5] Sun Y. Production of nitrogen and carbon S phases in austenitic stainless steels by hybrid plasma surface alloying. Surf Eng 2010;26(1–2):114–22.
[6] Czerwiec T, He H, Marcos G, Thiriet T, Weber S, Michel H. Fundamental and innovations in plasma assisted diffusion of nitrogen and carbon in austenitic stainless steels and related alloys. Plasma Process Polym 2009;6(6–7):401–9.
[7] Cheng Z, Li CX, Dong H, Bell T. Low temperature plasma nitrocarburizing of AISI 316 austenitic stainless steel. Surf Coat Technol 2005;191(2):195–200.
[8] Thaiwatthana S, Li XY, Dong H, Bell T. Comparison studies on properties of nitrogen and carbon S phase on low temperature plasma alloyed AISI 316 stainless steel. Surf Eng 2002;18(6):433–7.
[9] Spies H-J. Nitriding and nitrocarburizing. HTM J Heat Treat Mater 2013;68(2):86–96.
[10] Las Heras E, de Ybarra G, Lamas D, Cabo A, Dalibon EL, Brühl SP. Plasma nitriding of 316L stainless steel in two different N_2–H_2 atmospheres – influence on microstructure and corrosion resistance. Surf Coat Technol 2017;313:47–54.
[11] Fossati A, Borgioli F, Galvanetto E, Bacci T. Glow-discharge nitriding of AISI 316L austenitic stainless steel: influence of treatment time. Surf Coat Technol 2006;200(11):3511–7.
[12] Spies H-J, Eckstein C, Biermann H, Franke A. Corrosion behaviour of stainless steels after low temperature thermochemical treatment. Mat-wiss u Werkstofftech 2010;41(3):133–41.
[13] Mendes AF, Scheuer CJ, Joanidis IL, Cardoso RP, Mafra M, Klein AN, et al. Low-temperature plasma nitriding of sintered PIM 316L austenitic stainless steel. Mater Res 2014;17:100–9.
[14] Pye D. Practical nitriding and ferritic nitrocarburizing. Materials Park, OH: ASM International; 2003.
[15] Mahboubi F, Abdolvahabi K. The effect of temperature on plasma nitriding behaviour of DIN 1.6959 low alloy steel. Vacuum 2006;81(3):239–43.
[16] Maniee A, Mahboubi F, Soleimani R. The study of tribological and corrosion behavior of plasma nitrided 34CrNiMo6 steel under hot and cold wall conditions. Mater Des 2014;60:599–604.
[17] Heydarzadeh Sohi M, Ebrahimi M, Honarbakhsh Raouf A, Mahboubi F. Effect of plasma nitrocarburizing temperature on the wear behavior of AISI 4140 steel. Surf Coat Technol 2010;205:S84–9.
[18] Köster K, Kaestner P, Bräuer G, Hoche H, Troßmann T, Oechsner M. Material condition tailored to plasma nitriding process for ensuring corrosion and wear resistance of austenitic stainless steel. Surf Coat Technol 2013;228:S615–8.
[19] Alves C, da Silva EF, Martinelli AE. Effect of workpiece geometry on the uniformity of nitrided layers. Surf Coat Technol 2001;139(1):1–5.
[20] Olzon-Dionysio M, Campos M, Kapp M, de Souza S, de Souza SD. Influences of plasma nitriding edge effect on properties of 316L stainless steel. Surf Coat Technol 2010;204(21–22):3623–8.
[21] Li CX, Georges J, Li XY. Active screen plasma nitriding of austenitic stainless steel. Surf Eng 2002;18(6):453–7.
[22] Georges J. Nitriding process and nitriding furnace therefor, US Patent 5,989,363. 1999 Nov. 23. United States Patent No. 9,989,363. 1999 November 23.
[23] Spies H-J, Le Thien H, Biermann H. Verhalten von Stählen beim Plasmanitrieren mit einem Aktivgitter. HTM Härtereitechnische Mitteilungen 2005;60(4):240–7.
[24] Dalke A, Burlacov I, Hamann S, Puth A, Spies H-J, Röpcke J, et al. Plasma nitrocarburizing of AISI 316L austenitic stainless steel applying a carbon active screen: status and perspectives. HTM 2018;73(5):246–57.
[25] Dalke A, Burlacov I, Hamann S, Puth A, Böcker J, Spies H-J, et al. Solid carbon active screen plasma nitrocarburizing of AISI 316L stainless steel: Influence of N_2–H_2 gas composition on structure and properties of expanded austenite. Surf Coat Technol 2019;357:1060–8.
[26] Hubbard P, Dowey SJ, Doyle ED, McCulloch DG. Influence of bias and in situ cleaning on through cage (TC) or active screen plasma nitrided (ASPN) steels. Surf Eng 2006;22(4):243–7.
[27] Hubbard P, Dowey SJ, Partridge JG, Doyle ED, McCulloch DG. Investigation of nitrogen mass transfer within an industrial plasma nitriding system II: Application of a biased screen. Surf Coat Technol 2010;204(8):1151–7.
[28] Spies H-J, Burlacov I, Börner K, Biermann H. IFHTSE global 21: heat treatment and surface engineering in the twenty-first century active screen plasma nitriding and nitrocarburising of steels: an overview. Int Heat Treat Surf Eng 2014;8(3):94–106.
[29] Burlacov I, Hamann S, Spies H-J, Röpcke J, Biermann H. In-line process control in the active screen plasma nitrocarburizing using a combined approach based on infrared laser absorption spectroscopy and bias power management. HTM J Heat Treat Mater 2016;71(4):141–7.
[30] Burlacov I, Hamann S, Spies H-J, Dalke A, Röpcke J, Biermann H. A novel approach of plasma nitrocarburizing using a solid carbon active screen—a proof of concept. HTM 2017;72(5):254–9.
[31] Puth A, Hamann S, Kusýn L, Burlacov I, Dalke A, Spies H-J, et al. Spectroscopic investigations of plasma nitrocarburizing processes using an active screen made of carbon in a model reactor. Plasma Sources Sci Technol 2018;27(7):75017.
[32] Hamann S, Burlacov I, Spies H-J, Biermann H, Röpcke J. Spectroscopic investigations of plasma nitriding processes: a comparative study using steel and carbon as active screen materials. J Appl Phys 2017;121(15):153301.
[33] Puth A, Kusýn L, Pipa AV, Burlacov I, Dalke A, Hamann S, et al. Spectroscopic study of plasma nitrocarburizing processes with an industrial-scale carbon active screen. Plasma Sources Sci Technol 2020;29(3):35001.
[34] Wu D, Ge Y, Kahn H, Ernst F, Heuer AH. Diffusion profiles after nitrocarburizing austenitic stainless steel. Surf Coat Technol 2015;279:180–5.
[35] Jacob W, Hopf C, Schlüter M. Chemical sputtering of carbon by nitrogen ions. Appl Phys Lett 2005;86(20):204103.
[36] Schlüter M, Hopf C, Jacob W. Chemical sputtering of carbon by combined exposure to nitrogen ions and atomic hydrogen. New J Phys 2008;10(5):53037.
[37] Jaoul C, Belmonte T, Czerwiec T, David N. Nitrocarburizing treatments using flowing afterglow processes. Appl Surf Sci 2006;252(23):8360–6.
[38] Burlacov I, Börner K, Spies H-J, Biermann H, Lopatik D, Zimmermann H, et al. In-situ monitoring of plasma enhanced nitriding processes using infrared absorption and mass spectroscopy. Surf Coat Technol 2012;206(19):3955–60.
[39] Christiansen TL, Hummelshøj TS, Somers MAJ. Expanded austenite, crystallography and residual stress. Surf Eng 2010;26(4):242–7.

[40] Sun Y, Li XY, Bell T. X-ray diffraction characterisation of low temperature plasma nitrided austenitic stainless steels. J Mater Sci 1999;34(19):4793–802.
[41] Somers MAJ, Kücükyildiz ÖC, Ormstrup CA, Alimadadi H, Hattel JH, Christiansen TL, et al. Residual stress in expanded austenite on stainless steel; origin, measurement, and prediction. Mater Perf Charact 2018;7(4):20170145.
[42] Naeem M, Javed Iqbal M, Zakaullah M, Shafiq ZI, Mujahid JC, Díaz-Guillén, et al. Enhanced wear and corrosion resistance of AISI-304 steel by duplex cathodic cage plasma treatment. Surf Coat Technol 2019;375:34–45.
[43] Flis J. Corrosion and passivation of plasma nitrided stainless steels. Surf Eng 2010;26(1–2):103–13.
[44] Sun Y, Bell T, Kolosvary Z, Flis J. The response of austenitic stainless steels to low-temperature plasma nitriding. Heat Treat Met 1999;26:9–16.
[45] Spies H-J. 6 – Corrosion behaviour of nitrided, nitrocarburised and carburised steels. In: Mittemeijer EJ, Somers MAJ, editors. Thermochemical surface engineering of steels. Oxford: Woodhead Publishing; 2015. p. 267–309.